

Geophysical Research Letters

RESEARCH LETTER

10.1029/2018GL081544

Key Points:

- Magnetic perturbations seen during Europa flyby E26 consistent with Galileo's passage through a plume in the southern trailing hemisphere
- Interaction of the magnetospheric plasma with Europa's global exosphere alone is not sufficient to explain the observed magnetic field
- Combined with the detection of a plume during the earlier E12 flyby, this result suggests persistent plume activity during the Galileo era

Correspondence to:

H. Arnold,
hannes.arnold@eas.gatech.edu

Citation:

Arnold, H., Liuzzo, L., & Simon, S. (2019). Magnetic signatures of a plume at Europa during the Galileo E26 flyby. *Geophysical Research Letters*, 46, 1149–1157. <https://doi.org/10.1029/2018GL081544>

Received 3 DEC 2018

Accepted 28 JAN 2019

Accepted article online 31 JAN 2019

Published online 9 FEB 2019

Magnetic Signatures of a Plume at Europa During the Galileo E26 Flyby

Hannes Arnold¹ , Lucas Liuzzo¹ , and Sven Simon¹ 

¹School of Earth and Atmospheric Sciences, Georgia Institute of Technology, Atlanta, GA, USA

Abstract We analyze the magnetic field perturbations observed near Jupiter's icy moon Europa by the Galileo spacecraft during the E26 flyby on 3 January 2000. In addition to the expected large-scale signatures of magnetic fieldline draping and induction, the E26 data set contains various prominent structures on length scales much smaller than the moon's radius. By applying a hybrid (kinetic ions and fluid electrons) model of Europa's interaction with the impinging magnetospheric plasma, we demonstrate that these fine structures in the magnetic field are consistent with Galileo's passage through a water vapor plume whose source was located in Europa's orbital trailing, southern hemisphere. Considering the large-scale asymmetries of Europa's global atmosphere alone is not sufficient to explain the observed magnetic signatures. Combined with the recent identification of a plume during the earlier E12 flyby of Galileo, our results provide strong evidence that plume activity at Europa was a persistent phenomenon during the Galileo era.

Plain Language Summary Observations by the Hubble Space Telescope have revealed the presence of water vapor plumes at Jupiter's icy moon Europa. However, in contrast to the Enceladus plume, the occurrence of plumes at Europa seems to be a transient phenomenon. The mechanism governing the times and locations of these emissions is still unknown. In addition to telescope observations, magnetic field data collected near Europa can be applied as a tool to search for plumes. Since Europa is located within Jupiter's magnetosphere, the moon is continuously exposed to a flow of magnetized plasma with a relative velocity around 100 km/s. The interaction of this plasma with a plume at Europa will locally deflect the magnetospheric flow, thereby generating characteristic deformations of Jupiter's magnetic field. We have revisited magnetic field observations acquired by the Galileo spacecraft during its E26 flyby of Europa on 3 January 2000. By using a plasma simulation model, we demonstrate that the magnetic perturbations observed near Europa are indicative of a water vapor plume in the moon's trailing hemisphere. The source of this plume was located near the Butterdon Linea at Europa's surface. This finding is highly relevant for the planning of synergistic measurements during the upcoming Europa Clipper mission.

1. Introduction

The smallest Galilean moon, Europa (radius $R_E = 1,560.8$ km), likely hosts a global subsurface ocean (Kivelson et al., 2000). The thickness of the ocean is suspected to be on the order of 100 km (Schilling et al., 2007), whereas the estimates for the thickness of Europa's icy crust range from a few kilometers up to 60 km (Hand & Chyba, 2007; Hussmann et al., 2002; Schenk, 2002). Hubble Space Telescope (HST) observations in December 2012 revealed a localized increase of ultraviolet emission intensity near the south pole of Europa, associated with a surplus of oxygen and hydrogen. Roth et al. (2014a) demonstrated that the observed inhomogeneity in Europa's atmosphere could be interpreted as two water vapor plumes emanating near 180° W 75° S and 55° S, each with a scale height of about 200 km. A single, but broader, plume could explain the observations equally well. However, subsequent HST observations in 2014 and 2015 could not identify the anomalies observed in 2012, indicating that (in contrast to the Enceladean plumes), the plumes at Europa seem to be transient in nature (Roth et al., 2014b, 2016). Subsequently, Sparks et al. (2016, 2017) were able to find new, equatorial locations of enhanced neutral column density through image postprocessing of available HST data.

Europa orbits Jupiter at a distance of $9.38 R_J$ (radius of Jupiter $R_J = 71,492$ km). The moon is embedded in Jupiter's magnetosphere and its equatorial plasma sheet (Kivelson et al., 2009). Since the orbital period of Europa is significantly larger than Jupiter's rotational period (the synodic period is 11.23 hr with respect to

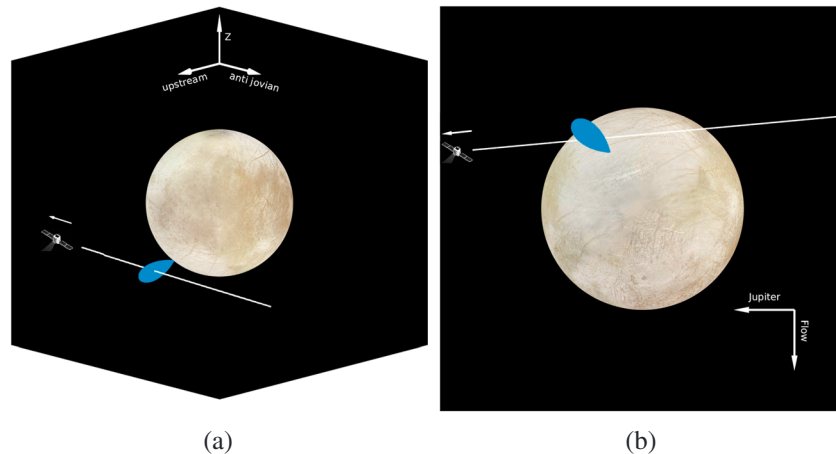


Figure 1. Geometry of the Galileo E26 flyby of Europa in EPhiO coordinates, as seen (a) from the upstream, Jupiter-averted side (b) when looking at the moon's southern hemisphere. The white line denotes the trajectory of the spacecraft. The blue isosurface illustrates the position and orientation of the plume included in simulation run #1 (see section 2 for details). The E26 trajectory is located within the $z \approx -0.8R_E$ plane of the EPhiO.

Europa), sub-Alfvénic, magnetospheric plasma continuously impinges onto Europa's tenuous atmosphere and ionosphere. The moon's ionosphere is mainly generated by electron impact ionization, with the contribution of solar ultraviolet ionization being an order of magnitude smaller (Saur et al., 1999). Mass loading of the magnetospheric plasma by Europa's ionosphere decelerates the impinging flow and deflects it around the moon (e.g., Rubin et al., 2015). The magnetospheric field drapes around the obstacle, forming Alfvén wings at larger distances to Europa (Neubauer, 1980, 1998).

Driven by the 9.6° tilt between Jupiter's magnetic and rotational axes, the ambient magnetospheric field near Europa exhibits an oscillation at Jupiter's synodic rotation period. This time variability induces a secondary magnetic field in Europa's conducting subsurface ocean, which has a dipolar shape outside of the moon (Khurana et al., 1998; Zimmer et al., 2000). Therefore, in addition to Europa's atmosphere/ionosphere, the magnetospheric plasma interacts with the (time-varying) dipole field induced in Europa's subsurface ocean (Kivelson et al., 1999). The induced dipole contributes to the plasma deflection and reduces the cross sections of the two Alfvénic fluxtubes, compared to a scenario without induction (Neubauer, 1999; Volwerk et al., 2007).

However, this picture considers only the influence of Europa's global atmosphere and induced field on the plasma interaction but not the impact of a possible plume. A localized inhomogeneity in the atmosphere generates a tube-like region of locally enhanced current density and flow deceleration within the main Alfvén wing, referred to as an *Alfvén winglet* by Blöcker et al. (2016). A plume source in, for example, Europa's southern hemisphere, will also break the symmetry of the Alfvén wings between the moon's northern and southern hemispheres (Blöcker et al., 2016). Due to the translational invariance along their characteristics Neubauer (1980), the Alfvén wings and associated asymmetries can extend to arbitrarily large distances from Europa. This facilitates a “remote” detection of plumes in magnetic field data from distant Europa flybys.

Out of the 12 Galileo flybys of Europa, only the E12 (on 16 December 1997) and E26 (on 3 January 2000) flybys passed at a low altitude of only 400 km to Europa's surface, an altitude of the same order as the scale height of the plume found by Roth et al. (2014a). Both of these flybys occurred in the orbital trailing hemisphere of Europa: The E12 flyby occurred at equatorial latitudes, whereas the E26 flyby occurred at more southern latitudes (see Figure 1). During E26, Europa was located at 03:00 local time and at a distance of $1.5 R_J$ below Jupiter's magnetospheric current sheet. As suggested by Blöcker et al. (2016), transverse currents within the plumes should leave a clear imprint in Galileo magnetometer data from such close flybys. Indeed, magnetic field observations from both flybys reveal sharp, highly localized perturbations in all three components near closest approach (C/A) of the spacecraft that are superimposed on the signatures of the main Alfvén wings.

The black lines in Figure 2 display magnetometer data from the E26 flyby in EPhiO coordinates. In this Cartesian coordinate system, the x axis is aligned with the corotational flow direction, the y axis points toward Jupiter, and the z axis completes the right-handed system. The origin of the EPhiO system coin-

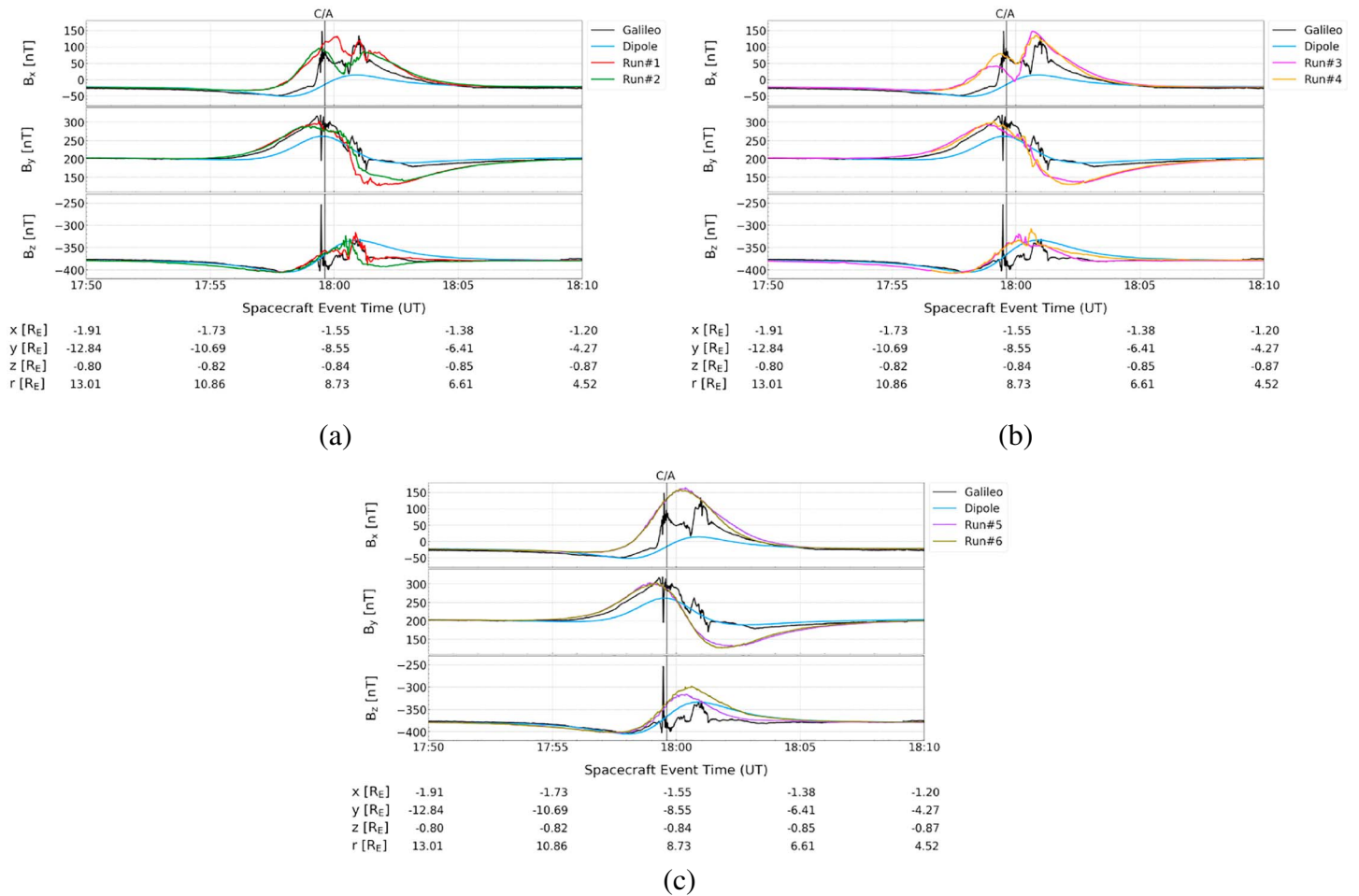


Figure 2. Modeled and measured magnetic field along the E26 trajectory. (a–c) Each of the three panels illustrates the magnetic field components observed by Galileo (black) as well as the dipolar magnetic field associated with induction in Europa’s subsurface ocean alone (light blue). In addition, the modeled magnetic fields from two of the hybrid simulation runs are shown in each panel. To facilitate the identification of fine structures in the magnetic field, each panel contains only the results of two simulations. The vertical black line denotes Galileo’s closest approach to Europa at 17:59:37. C/A = closest approach.

cides with the center of Europa. The B_x component observed during E26 shows a broad enhancement between 17:59:00 and 18:05:00, associated with the bending of the field toward downstream in the southern Alfvén wing. Superimposed on the main Alfvén wing signature is a double-peak structure (between 17:59:30 and 18:01:00) with a magnitude of about $B_x = 150$ nT at the two spikes and a minimum of $B_x = 25$ nT in between the enhancements. The observed perturbation in the B_y component mainly consists of a single, prominent enhancement of 100 nT near 18:01:00. The B_z component shows multiple drops and enhancements during the same interval as B_x .

Blöcker et al. (2016) applied a three-dimensional magnetohydrodynamic model with a single plume in Europa’s southern trailing hemisphere to investigate whether the magnetic perturbations measured during E26 could contain any hints of plume activity during the flyby. With this model, Blöcker et al. (2016) were able to qualitatively reproduce the outbound enhancement in B_x . However, their model severely underestimated the magnitude of the B_x peak in the inbound region. Also, the width of the modeled B_x peak in the outbound region was much larger than observed by Galileo. The model of Blöcker et al. (2016) could not reproduce the observed B_y enhancement between 17:56:00 and 18:02:00. The perturbations in the observed B_z component could not be matched in magnitude nor structure. Blöcker et al. (2016) ascribed the discrepancies between model and observations to the missing ionospheric Hall effect and the radially symmetric atmospheric density profile applied in their model. Their model was therefore unable to determine whether or not Galileo had passed through a plume during the E26 encounter. Several other models tried to explain the magnetic field data from the E26 flyby without inclusion of a local plume source (Rubin et al., 2015;

Schilling et al., 2008). While these studies were able to describe the magnitude of the broad B_x enhancement associated with the southern Alfvén wing crossing (during 17:59:00–18:05:00), they did not succeed in explaining the double-peaked fine structure within the Alfvén wing.

Magnetic field data from the E12 flyby display similarly localized perturbations on a scale smaller than the radius of Europa. Using the BATS-R-US multifluid magnetohydrodynamic model, Jia et al. (2018) searched for plume signatures in magnetic field and plasma data from the E12 encounter. These authors were able to attribute the observed sharp enhancements and drops in all three magnetic field components over a distance of 1,000 km near C/A to a plume at Europa. However, the model of Jia et al. (2018) underestimated the observed amplitudes of the perturbations in B_x and B_y by more than a factor of 2. The density enhancement observed by the Galileo Plasma Wave Spectrometer near C/A was reproduced by the model of Jia et al. (2018). However, the structures in the plasma density observed in the outbound region were not matched by their simulation. Overall, Jia et al. (2018) provided strong evidence that the location and extension of the magnetic field and plasma perturbations observed during the E12 flyby were generated by a plume.

Building upon the work of Blöcker et al. (2016) and the recent, successful plume identification by Jia et al. (2018), the goal of our study is to search Galileo magnetic field data from E26 for evidence of a plume in Europa's orbital trailing, southern hemisphere.

2. Model Description

We apply the AIKEF (Adaptive Ion-Kinetic Electron-Fluid) hybrid code (Müller et al., 2011) for our simulations, which treats ions as particles and electrons as a massless, charge-neutralizing fluid. In contrast to the magnetohydrodynamic approach of Schilling et al. (2008) and Blöcker et al. (2016), AIKEF can describe asymmetries in the plasma flow due to the ionospheric Hall effect as well as flow shear between the magnetospheric plasma and the plasma emanating from Europa (e.g., from its ionosphere or a plume source). AIKEF has already been successfully applied to model Cassini magnetic field observations from multiple flybys through the Enceladus plume (Kriegel et al., 2014, 2011, 2009).

We use similar magnetospheric upstream parameters as Rubin et al. (2015) and Blöcker et al. (2016) to facilitate a comparison to their results for the E26 flyby. Since the bulk velocity of the (nearly) corotating plasma relative to Europa is not constrained through observations from E26, we use a value of $u_0 = 100$ km/s in agreement with Bagenal et al. (2015). The upstream number density in the simulations ($n = 30 \cdot 10^6 \text{ m}^{-3}$) is consistent with the range of values measured by Galileo during the flyby (Kurth et al., 2001). The plasma density during E26 was about a factor of 20 smaller than the anomalously high density observed during E12 (Kurth et al., 2001), suggesting a much weaker plasma interaction during E26. For the average mass of the incident, singly charged ions we use $m_i = 18.5$ amu (Kivelson et al., 2004). The temperature of the impinging ions and electrons is set to the same value of $k_B T_{i,e} = 100$ eV (Kivelson et al., 2004) and the magnetospheric background field during the E26 flyby is $\vec{B}_0 = (-22, 205, -379)$ nT (see Kivelson et al., 1999, and Figure 2). These parameters result in an Alfvénic Mach number for the upstream plasma of $M_A = 0.25$.

Due to the vast difference in the timescales of the plasma interaction and induction effects (minutes compared to hours, see Seufert et al., 2011), the field induced in Europa's subsurface ocean during the E26 flyby can be represented in our model as a static dipole moment (Neubauer, 1999; Zimmer et al., 2000). In analogy to Rubin et al. (2015), Europa's interior is treated as a perfectly conducting sphere (see also Kivelson et al., 1999; Zimmer et al., 2000, for details).

In our model, Europa's atmosphere consists of molecular oxygen, which was found to be the dominant species (Hall et al., 1995; McGrath et al., 2009). Sputtering of Europa's surface is not uniform: Pospieszalska and Johnson (1989) as well as Cassidy et al. (2013) showed that the sputtering rate decreases from the trailing hemisphere toward the leading hemisphere. Therefore, for the neutral density distribution, we use an analytical description similar to the model of Rubin et al. (2015). The density profile in the trailing n_T and leading n_L hemispheres reads

$$\begin{aligned} n_L(h) &= n_0 \cdot \exp\left(-\frac{h}{h_0}\right), & 90^\circ < \alpha \leq 180^\circ, \\ n_T(h, \alpha) &= n_L(h) \cdot (1 + A \cdot \cos(\alpha)), & \alpha \leq 90^\circ, \end{aligned} \quad (1)$$

with the radial distance $h = |\vec{r}| - R_E$ (where \vec{r} is the position vector from Europa's center) to Europa's surface, the neutral scale height $h_0 = 50$ km, and the surface density $n_0 = 1 \cdot 10^{14} \text{ m}^{-3}$. The symbol α denotes the

angle between the position \vec{r} and the negative x axis (which points into the trailing/ramside hemisphere). The parameter A represents the strength of the trailing/leading asymmetry. We consider two cases: $A = 0$, similar to the symmetric, barometric profile of Blöcker et al. (2016) and $A = 10$. In this way, we can systematically assess the potential of large-scale/global atmospheric asymmetries to obstruct any (locally) observable plume signatures in the magnetic field. The O_2 column density in our runs therefore ranges from $5.5 \cdot 10^{19} \text{ m}^{-2}$ for $A = 10$ to $5 \cdot 10^{18} \text{ m}^{-2}$ for $A = 0$, consistent with the interval of $10^{18} - 10^{19} \text{ m}^{-2}$ inferred from HST observations (Hall et al., 1995; Plainaki et al., 2018; Saur et al., 1998).

We also consider a single water vapor plume with the neutral density profile suggested by Jia et al. (2018):

$$n_P(h, \Delta\theta) = n_{P,0} \cdot \exp \left[- \left(\frac{h}{h_p} \right)^2 - \left(\frac{\Delta\theta(\vec{P})}{h_\theta} \right)^2 \right], \quad (2)$$

where $\Delta\theta(\vec{P})$ represents the angular distance from the plume axis \vec{P} (which is *not* necessarily perpendicular to Europa's surface), h_p the scale height of the plume, h_θ the opening angle of the plume, and $n_{P,0}$ the surface number density of the plume. Thus, the neutral density profile of the plume is rotationally symmetric around the plume axis \vec{P} . In our simulations, we use $h_p = 200 \text{ km}$, $h_\theta = 15^\circ$, and $n_{P,0} = 3.9 \cdot 10^{15} \text{ m}^{-3}$, resulting in a column density of H_2O along the plume axis of $7.8 \cdot 10^{20} \text{ m}^{-2}$. This value is consistent with the range of values inferred from HST observations: $1.5 \cdot 10^{20} \text{ m}^{-2}$ (Roth et al., 2014a) to $2.3 \cdot 10^{21} \text{ m}^{-2}$ (Sparks et al., 2016). The location of the plume's "footpoint" and orientation of its symmetry axis \vec{P} with respect to the surface are free parameters in our model. However, we place its footpoint in the vicinity of the Butterdon Linea (see Table 1 of Doggett et al., 2009), which is the surface feature closest to the E26 trajectory. Assuming that the generation mechanism of plumes on Europa is similar to that of the plumes at Enceladus (Porco et al., 2006), we allow an inclination of the plume axis \vec{P} against the local radial/zenith direction at its footpoint (see Jia et al., 2018). The footpoint of the plume at Europa's surface is located at

$$\vec{F}(\theta_F, \phi_F) = R_E(\sin(\theta_F) \cos(\phi_F), \sin(\theta_F) \sin(\phi_F), \cos(\theta_F)), \quad (3)$$

where ϕ_F is measured in the right-handed EPhiO coordinates, whereas $\theta_F = 0^\circ$ marks Europa's north pole and $\theta_F = 180^\circ$ Europa's south pole, respectively. The inclination of the plume axis \vec{P} against the local radial direction at the footpoint \vec{F} is defined by the angles $\tilde{\theta} = \theta - \theta_F$ and $\tilde{\phi} = \phi - \phi_F$, that is, $\tilde{\theta} = 0^\circ$, $\tilde{\phi} = 0^\circ$ means that the plume axis \vec{P} is perpendicular to the surface. We have carried out multiple simulation runs for various combinations of footpoint locations and orientations of the plume axis. The following four sets of parameters were found to yield best possible agreement between modeled and measured magnetic field perturbations: run #1: $A = 10$, $\vec{P}(\theta, \phi, \tilde{\theta}, \tilde{\phi}) = (140^\circ, 300^\circ, -20^\circ, -20^\circ)$; run #2: $A = 10$, $\vec{P}(\theta, \phi, \tilde{\theta}, \tilde{\phi}) = (140^\circ, 300^\circ, 0^\circ, -10^\circ)$; run #3: $A = 10$, $\vec{P}(\theta, \phi, \tilde{\theta}, \tilde{\phi}) = (140^\circ, 300^\circ, 0^\circ, 35^\circ)$; and run #4: $A = 10$, $\vec{P}(\theta, \phi, \tilde{\theta}, \tilde{\phi}) = (135^\circ, 305^\circ, 0^\circ, 35^\circ)$. For reference, we have also carried out two simulations *without* a plume, using an asymmetric atmosphere ($A = 10$) in run #5 and a symmetric atmosphere ($A = 0$, with a higher base density of $11 \cdot n_0$, to compare it with run #5) in run #6.

In our model, the neutral atmosphere and plume are ionized by electron impacts, which is the dominant ionization process at Europa (Saur et al., 1998). In analogy to Blöcker et al. (2016), Schilling et al. (2008), and Jia et al. (2018), we calculate the ion production rate by multiplying the electron impact ionization rate $f_{\text{imp}}(T_e)$ for H_2O and O_2 with the respective neutral density profile. To derive the electron impact ionization rate of each species, we assume a Maxwellian velocity distribution for the ionizing electrons and integrate over their energy-dependent ionization cross sections (taken from the National Institute of Standards and Technology database [Kim et al., 2004]); see also the approach of Banks and Kockarts (1973). This leads to constant ionization rates of $2 \cdot 10^{-6} \text{ s}^{-1}$ for H_2O^+ and $2.3 \cdot 10^{-6} \text{ s}^{-1}$ for O_2^+ . The assumption of a *constant* ionization rate is consistent with the approach of Blöcker et al. (2016) and Jia et al. (2018). Our model also considers loss of ionospheric O_2^+ and H_2O^+ ions due to dissociative recombination, with the recombination rates given in Schunk and Nagy (2000):

$$\begin{aligned} \alpha_{O_2^+} &= 2 \cdot 10^{-13} \left(\frac{300}{T_e} \right)^{0.7} \text{ m}^3/\text{s}, \\ \alpha_{H_2O^+} &= 1.03 \cdot 10^{-9} (T_e)^{-1.111} \text{ m}^3/\text{s}. \end{aligned} \quad (4)$$

The extensions of our simulation domain are $-10R_E \leq x \leq 20R_E$, $-15R_E \leq y \leq 15R_E$, and $-30R_E \leq z \leq 30R_E$. The grid resolution varies between three regions of our simulation box (centered around (0,0,0)):

33 km for $|x, y, z| \leq 1.5R_E$, 66 km for $1.5R_E < |x, y, z| \leq 3R_E$, and 132 km outside of that cube. Analogous to the approach of Blöcker et al. (2016), we discontinue the simulations as soon as the Alfvén wings reach the outer boundaries of the domain.

3. Results

In Figures 2a–2c, the comparison between the modeled (runs #1 to #6 from section 2) and measured magnetic field signatures (black lines) is depicted. For reference, we also show the dipolar field induced in the subsurface ocean (without any contributions from plasma currents, light blue line) in all panels.

The B_x component in all six runs shows a broad enhancement between 17:57:00 and 18:04:00, corresponding to the crossing of the southern Alfvén wing, similar to the results of Schilling et al. (2007), Rubin et al. (2015), and Blöcker et al. (2016). Runs #1 to #4 (which include a plume) also reveal the prominent double-peak feature in B_x between 17:59:30 and 18:01:00. The relative strength of the two enhancements varies between our simulations. Runs #3 and #4 display a weaker inbound (18:00:00) than outbound peak (18:01:30) in B_x , whereas the magnitude and shape of the two peaks in run #2 are nearly symmetric around the local minimum (18:00:30). In run #1, the inbound enhancement in B_x is about 10 nT stronger than the outbound enhancement. The fine structure of the B_x signature observable along the E26 trajectory is highly sensitive to even slight changes in the orientation and footpoint of the plume axis \vec{P} . However, the width of the modeled B_x signature in all four runs with a plume is consistent with the Galileo data.

All six model runs produce a bipolar perturbation in the B_y component: An enhancement in the inbound region is followed by a decrease in the outbound region. Comparison to the pure induction signal (light blue line) illustrates that the inbound B_y signature is generated when the dipole field is compressed by the plasma interaction, thereby amplifying the perturbations associated with an induced dipole field alone. The magnitude and width of the B_y enhancement observed in the inbound region are well reproduced by all six model runs. However, compared to observations, the contribution of plasma currents is overestimated in the outbound region. All other models that have been applied to E26 without a plume (Rubin et al., 2015; Schilling et al., 2007) as well as with a plume (Blöcker et al., 2016) produced a similar outbound depletion in B_y as our model. The discrepancy in the outbound region of B_y may be caused by a locally enhanced current density within the plume that is not reproduced by the analytical density profile applied here (equation (2)). An analysis of the two-dimensional magnetic field structures in the E26 flyby plane (Figure 3, see below) will shed additional light on the origin of this structure. If a plume is considered, only the sharp flank between the inbound and outbound signatures in B_y (17:59:00–18:00:01) changes quantitatively. The modeled B_y component therefore contains the least indicative signatures for the presence of a plume.

The observed B_z component displays a bipolar structure as well: An enhanced $|B_z|$ was detected by Galileo in the inbound region (17:51:00–17:59:30), followed by a decrease in the outbound region immediately after 17:59:30. The inbound enhancement of $|B_z|$ is nearly identical to the pure induction signal, indicating that plasma currents made only a weak contribution to this feature. The width and magnitude of the inbound $|B_z|$ increase are well reproduced by all six hybrid runs. The B_z perturbation observed outbound is highly localized: It possesses an extension of only $0.1R_E$ along the flyby trajectory (crossed between 18:01:00 and 18:02:00) and is bounded by discontinuity-like jumps of B_z on both sides. Furthermore, the location of the outbound depression in $|B_z|$ nearly coincides with the outbound spike seen in B_x (which could clearly be associated with Galileo's passage through a plume). The model's ability to reproduce the pillar-like outbound depletion of $|B_z|$ near 18:01:00 strongly depends on the plume orientation and location of its footpoint: Even slight changes of either lead to a drastic change of width and magnitude of the modeled B_z structure (e.g., run #1 versus run #4). The best agreement in both, width and magnitude of the outbound B_z feature is achieved in run#1: In this case, model and observation are nearly indistinguishable. The model used by Blöcker et al. (2016) was not able to reproduce the observed orientation of B_z *anywhere* in the perturbed segment.

In conclusion, each of the four runs reproduces certain features of the observed magnetic field components better than the other three. Therefore, we refrain from choosing a “best fit” run.

For comparison, Figure 2c displays the modeled magnetic field signatures for the case of an asymmetric (run #5) and symmetric (run #6) global atmosphere but *without* a plume included. Neither of these runs is able to reproduce any of the magnetic fine structures observed by Galileo around closest approach, consistent with the modeling results of Schilling et al. (2008) and Rubin et al. (2015; see Figure 10 in both works).

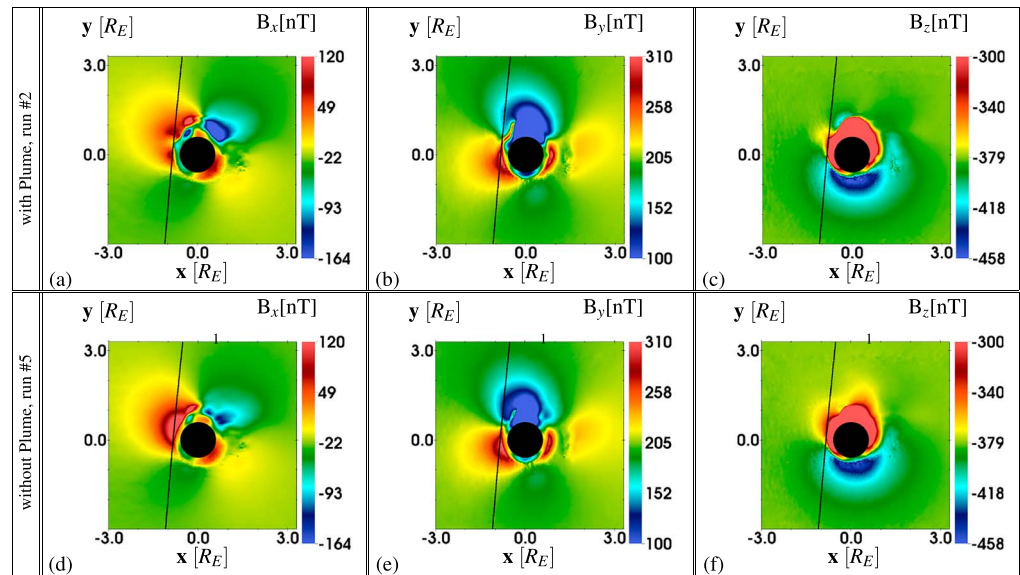


Figure 3. Two-dimensional illustration of the magnetic field components (B_x, B_y, B_z) close to Galileo's E26 flyby, in the plane of $z = -0.8R_E$. For a scenario with (run #2, panels a–c) and without (run #5, panels d–f) a plume, the figure illustrates Europa's magnetic environment near the E26 trajectory. The solid black lines indicate the flyby trajectory.

This provides strong additional evidence that the magnetic signatures observed around closest approach of E26 were (partially) generated by a localized atmospheric inhomogeneity with an extension much smaller than Europa. A comparison of the magnetic signatures from runs #5 and #6 also indicates that a global ram/wake asymmetry of Europa's atmosphere makes only minor quantitative contributions to the magnetic field signatures observable upstream of the moon: It mainly affects the B_z signatures in the outbound region.

Figure 3 shows two-dimensional cuts through the magnetic field near the flyby plane at $z = -0.8R_E$. Results are displayed for run #2 (plume included, panels a–c) and run #5 (no plume, panels d–f). Note that the background field \vec{B}_0 is not parallel to any plane of the EPhiO coordinate system.

In the model results with the plume included (see Figure 3a), the B_x component exhibits three distinct signatures along the trajectory: the two enhanced (dark red) outer segments of the double-peak structure and the narrow region in between (orange/yellow), where B_x is reduced compared to the peak values at the spikes. A similar B_x depletion occurs in all four runs with a plume included. In the run without the plume (see Figure 3d), the region of reduced B_x is moved closer to Europa because the local bulge in the field generated by the plume is no longer present. Changes due to a plume in the overall B_x topology are rather subtle and occur on length scales much smaller than Europa's radius. Therefore, if the spacecraft trajectory during the E26 flyby were only slightly displaced, an unambiguous identification of a local plume source may have been severely complicated.

For B_y (see Figures 3b and 3e), the model displays only minor quantitative differences between both cases, which is consistent with the results obtained along the flyby trajectory (see Figure 2). It is important to note that Figure 3b displays a “finger-like,” narrow region of enhanced B_y (depicted in dark red and yellow) along the outbound segment of the E26 trajectory. This enhancement locally interrupts the extended region of negative B_y perturbation in the Jupiter-facing hemisphere associated with field line draping. A slightly different plume orientation or a slightly different shape of the neutral gas profile may shift this feature closer to the path of the spacecraft, thereby eliminating large portions of the outbound decrease in B_y visible in our simulations. Using the plume model from equation (2), we did not find a parameter set that *simultaneously* explains B_x and B_z as well as the observed, weak dip in the outbound segment of B_y . However, our results clearly indicate that a plume source may indeed generate a highly localized channel through the region of reduced B_y , along which Galileo may have traveled during the E26 flyby. Due to the uncertainties in the upstream conditions (especially the bulk velocity of the incident magnetospheric flow during E26 is not well constrained) and the numerous degrees of freedom in the shape and orientation of the plume model, the

parameter space to be explored for improving agreement in the outbound segment of B_y is vast. This effort is beyond the scope of the present study.

Figures 3c and 3f depict two-dimensional cuts through the modeled B_z component. In the Jupiter-averted hemisphere ($y < 0$), we see an extended region of enhanced $|B_z|$, associated with the induced dipole alone. In the Jupiter-facing hemisphere, the region of locally reduced $|B_z|$ (which is strongly shaped by plasma currents) is slightly different between Figures 3c and 3f. Galileo just “scratched” the outer regions of this structure. In the run with a plume included, the outbound B_z feature is more confined, which explains the localized, narrow “pillar” visible in both the modeled and the observed magnetic field time series.

4. Concluding Remarks

Our model shows that a plume source is required to explain the fine structures in the magnetic field perturbations observed by Galileo during the E26 flyby of Europa. The modeled magnetic signatures along the E26 trajectory are highly sensitive to the plume orientation and the location of the plume’s footpoint at Europa’s surface. Multiple sets of plume parameters were found to be in similarly good agreement with observations. It is therefore not feasible to quantitatively constrain parameters of the plume (e.g., the neutral gas content or shape) based on magnetic field observations alone. In addition to the E12 flyby (Jia et al., 2018), E26 has become the second Galileo encounter with a strong indication of plume activity. Although yet unnoticed, plumes at Europa seem to have been a persistent phenomenon during the Galileo area.

Acknowledgments

The authors are grateful to the National Aeronautics and Space Administration (NASA) for financial support of this project through the *Solar System Workings 2016* program, grant 80NSSC17K0772. Galileo magnetic field data have been obtained from the *Planetary Data System*. Results from the AIKEF hybrid model and figures presented in this publication can be downloaded at <https://github.com/harnold8/E26> or obtained from the corresponding author upon request.

References

- Bagenal, F., Sidrow, E., Wilson, R. J., Cassidy, T. A., Dols, V., Cray, F. J., et al. (2015). Plasma conditions at Europa’s orbit. *Icarus*, *261*, 1–13. <https://doi.org/10.1016/j.icarus.2015.07.036>
- Banks, P. M., & Kockarts, G. (1973). *Aeronomy*, part A. (p. 184). San Diego, CA: Academic.
- Blöcker, A., Saur, J., & Roth, L. (2016). Europa’s plasma interaction with an inhomogeneous atmosphere: Development of Alfvén winglets within the Alfvén wings. *Journal of Geophysical Research: Space Physics*, *121*, 9794–9828. <https://doi.org/10.1002/2016JA022479>
- Cassidy, T. A., Paranicas, C. P., Shirley, J. H., Dalton, J. B. III, Teolis, B. D., Johnson, R. E., et al. (2013). Magnetospheric ion sputtering and water ice grain size at Europa. *Planetary and Space Science*, *77*, 64–73. <https://doi.org/10.1016/j.pss.2012.07.008>
- Doggett, T., Greeley, R., Figueredo, P., & Tanaka, K. (2009). Geologic Stratigraphy and Evolution of Europa’s Surface. In R. T. Pappalardo, W. B. McKinnon, & K. K. Khurana (Eds.), *Europa* (137 pp.). Tucson, AZ: University of Arizona Press.
- Hall, D. T., Strobel, D. F., Feldman, P. D., McGrath, M. A., & Weaver, H. A. (1995). Detection of an oxygen atmosphere on Jupiter’s moon Europa. *Nature*, *373*, 677–679. <https://doi.org/10.1038/373677a0>
- Hand, K. P., & Chyba, C. F. (2007). Empirical constraints on the salinity of the European ocean and implications for a thin ice shell. *Icarus*, *189*(2), 424–438. <https://doi.org/10.1016/j.icarus.2007.02.002>
- Hussmann, H., Spohn, T., & Wiczerkowski, K. (2002). Thermal equilibrium states of Europa’s ice shell: Implications for internal ocean thickness and surface heat flow. *Icarus*, *156*(1), 143–151. <https://doi.org/10.1006/icar.2001.6776>
- Jia, X., Kivelson, M. G., Khurana, K. K., & Kurth, W. S. (2018). Evidence of a plume on Europa from Galileo magnetic and plasma wave signatures. *Nature Astronomy*, *2*, 459–464. <https://doi.org/10.1038/s41550-018-0450-z>
- Khurana, K. K., Kivelson, M. G., Stevenson, D. J., Schubert, G., Russell, C. T., Walker, R. J., & Polanskey, C. (1998). Induced magnetic fields as evidence for subsurface oceans in Europa and Callisto. *Nature*, *395*(6704), 777–780. <https://doi.org/10.1038/27394>
- Kim, Y.-K., Irikura, M., ans Rudd, K. K., Ali, M., & Stone, P. (2004). Electron-impact cross sections for ionization and excitation database. NIST Standard Reference Database 107 (ver. 3.0), <https://doi.org/10.18434/T4KK5C>
- Kivelson, M. G., Bagenal, F., Kurth, W. S., Neubauer, F. M., Paranicas, C., & Saur, J. (2004). Magnetospheric interactions with satellites. In M. G. Kivelson et al. (Eds.), *Jupiter: The planet, satellites and magnetosphere* (pp. 513–536). Cambridge: Cambridge University Press.
- Kivelson, M. G., Khurana, K. K., Russell, C. T., Volwerk, M., Walker, R. J., & Zimmer, C. (2000). Galileo magnetometer measurements: A stronger case for a subsurface ocean at Europa. *Science*, *289*, 1340–1343. <https://doi.org/10.1126/science.289.5483.1340>
- Kivelson, M. G., Khurana, K. K., Stevenson, D. J., Bennett, L., Joy, S., Russell, C. T., et al. (1999). Europa and Callisto: Induced or intrinsic fields in a periodically varying plasma environment. *Journal of Geophysical Research*, *104*(A3), 4609–4626. <https://doi.org/10.1029/1998JA900095>
- Kivelson, M. G., Khurana, K. K., & Volwerk, M. (2009). Europa’s interaction with the Jovian magnetosphere. in *Europa*, edited by Robert T. Pappalardo, William B. McKinnon, Krishan K. Khurana; with the assistance of René Dotson with 85 collaborating authors. University of Arizona Press, Tucson, 2009. The University of Arizona space science series ISBN: 9780816528448, p.545, p. 545.
- Kriegl, H., Simon, S., Meier, P., Motschmann, U., Saur, J., Wennmacher, A., et al. (2014). Ion densities and magnetic signatures of dust pick-up at Enceladus. *Journal of Geophysical Research: Space Physics*, *119*, 2740–2774. <https://doi.org/10.1002/2013JA019440>
- Kriegl, H., Simon, S., Motschmann, U., Saur, J., Neubauer, F., Persoon, A., et al. (2011). Influence of negatively charged plume grains on the structure of Enceladus’ Alfvén wings: Hybrid simulations versus Cassini magnetometer data. *Journal of Geophysical Research*, *116*, A10223. <https://doi.org/10.1029/2011JA016842>, cited By 41.
- Kriegl, H., Simon, S., Müller, J., Motschmann, U., Saur, J., Glassmeier, K.-H., & Dougherty, M. (2009). The plasma interaction of enceladus: 3D hybrid simulations and comparison with Cassini MAG data. *Planetary and Space Science*, *57*(14), 2113–2122. <https://doi.org/10.1016/j.pss.2009.09.025>
- Kurth, W., Gurnett, D., Persoon, A., Roux, A., Bolton, S., & Alexander, C. (2001). The plasma wave environment of Europa. *Planetary and Space Science*, *49*(3), 345–363. [https://doi.org/10.1016/S0032-0633\(00\)00156-2](https://doi.org/10.1016/S0032-0633(00)00156-2), magnetospheres of the Outer Planets (Part I).
- McGrath, M. A., Hansen, C. J., & Hendrix, A. R. (2009). Observations of Europa’s tenuous atmosphere. in *Europa*, Edited by Robert T. Pappalardo, William B. McKinnon, Krishan K. Khurana; with the assistance of René Dotson with 85 collaborating authors. University

- of Arizona Press, Tucson, 2009. The University of Arizona space science series ISBN: 9780816528448, p.485, edited by R. T. Pappalardo, W. B. McKinnon, and K. K. Khurana, p. 485.
- Müller, J., Simon, S., Motschmann, U., Schüle, J., Glassmeier, K., & Pringle, G. J. (2011). A.I.K.E.F.: Adaptive hybrid model for space plasma simulations. *Computer Physics Communications*, *182*(4), 946–966. <https://doi.org/10.1016/j.cpc.2010.12.033>
- Neubauer, F. M. (1980). Nonlinear standing Alfvén wave current system at Io: Theory. *Journal of Geophysical Research*, *85*, 1171–1178. <https://doi.org/10.1029/JA085iA03p01171>
- Neubauer, F. M. (1998). The sub-Alfvénic interaction of the Galilean satellites with the Jovian magnetosphere. *Journal of Geophysical Research*, *103*, 19,843–19,866. <https://doi.org/10.1029/97JE03370>
- Neubauer, F. M. (1999). Alfvén wings and electromagnetic induction in the interiors: Europa and Callisto. *Journal of Geophysical Research*, *104*, 28,671–28,684. <https://doi.org/10.1029/1999JA900217>
- Plainaki, C., Cassidy, T. A., Shematovich, V. I., Milillo, A., Wurz, P., Vorburger, A., et al. (2018). Towards a global unified model of Europa's tenuous atmosphere. *Space Science Reviews*, *214*(1), 40. <https://doi.org/10.1007/s11214-018-0469-6>
- Porco, C. C., Helfenstein, P., Thomas, P. C., Ingersoll, A. P., Wisdom, J., West, R., et al. (2006). Cassini observes the active south pole of Enceladus. *Science*, *311*(5766), 1393–1401. <https://doi.org/10.1126/science.1123013>
- Pospieszalska, M. K., & Johnson, R. E. (1989). Magnetospheric ion bombardment profiles of satellites—Europa and Dione. *Icarus*, *78*, 1–13. [https://doi.org/10.1016/0019-1035\(89\)90065-1](https://doi.org/10.1016/0019-1035(89)90065-1)
- Roth, L., Retherford, K. D., Saur, J., Strobel, D. F., Feldman, P. D., McGrath, M. A., & Nimmo, F. (2014b). Orbital apocenter is not a sufficient condition for HST/STIS detection of Europa's water vapor aurora. *Proceedings of the National Academy of Science*, *111*, E5123–E5132. <https://doi.org/10.1073/pnas.1416671111>
- Roth, L., Retherford, K. D., Saur, J., Strobel, D. F., Feldman, P. D., McGrath, M. A., & Nimmo, F. (2014a). Transient water vapor at Europa's south pole. *Science*, *343*(6167), 171–174. <https://doi.org/10.1126/science.1247051>
- Roth, L., Saur, J., Retherford, K. D., Strobel, D. F., Feldman, P. D., McGrath, M. A., et al. (2016). Europa's far ultraviolet oxygen aurora from a comprehensive set of HST observations. *Journal of Geophysical Research: Space Physics*, *121*, 2143–2170. <https://doi.org/10.1002/2015JA022073>
- Rubin, M., Jia, X., Altwegg, K., Combi, M. R., Daldorff, L. K. S., Gombosi, T. I., et al. (2015). Self-consistent multifluid MHD simulations of Europa's exospheric interaction with Jupiter's magnetosphere. *Journal of Geophysical Research: Space Physics*, *120*, 3503–3524. <https://doi.org/10.1002/2015JA021149>
- Saur, J., Neubauer, F. M., Strobel, D. F., & Summers, M. E. (1999). Three-dimensional plasma simulation of Io's interaction with the Io plasma torus: Asymmetric plasma flow. *Journal of Geophysical Research*, *104*(A11), 25,105–25,126. <https://doi.org/10.1029/1999JA900304>
- Saur, J., Strobel, D. F., & Neubauer, F. M. (1998). Interaction of the Jovian magnetosphere with Europa: Constraints on the neutral atmosphere. *Journal of Geophysical Research*, *103*, 19,947–19,962. <https://doi.org/10.1029/97JE03556>
- Schenk, P. M. (2002). Thickness constraints on the icy shells of the Galilean satellites from a comparison of crater shapes. *Nature*, *417*, 419–421.
- Schilling, N., Neubauer, F. M., & Saur, J. (2007). Time-varying interaction of Europa with the Jovian magnetosphere: Constraints on the conductivity of Europa's subsurface ocean. *Icarus*, *192*(1), 41–55. <https://doi.org/10.1016/j.icarus.2007.06.024>
- Schilling, N., Neubauer, F. M., & Saur, J. (2008). Influence of the internally induced magnetic field on the plasma interaction of Europa. *Journal of Geophysical Research*, *113*, A03203. <https://doi.org/10.1029/2007JA012842>
- Schunk, R. W., & Nagy, A. F. (2000). *Ionospheres: Physics, plasma physics, and chemistry*. Cambridge: Cambridge University Press.
- Seufert, M., Saur, J., & Neubauer, F. M. (2011). Multi-frequency electromagnetic sounding of the Galilean moons. *Icarus*, *214*(2), 477–494. <https://doi.org/10.1016/j.icarus.2011.03.017>
- Sparks, W. B., Hand, K. P., McGrath, M. A., Bergeron, E., Cracraft, M., & Deustua, S. E. (2016). Probing for evidence of plumes on Europa with HST/STIS. *The Astrophysical Journal*, *829*(2), 121.
- Sparks, W. B., Schmidt, B. E., McGrath, M. A., Hand, K. P., Spencer, J. R., Cracraft, M., & Deustua, S. E. (2017). Active cryovolcanism on Europa? *The Astrophysical Journal Letters*, *839*(2), L18.
- Volwerk, M., Khurana, K., & Kivelson, M. (2007). Europa's Alfvén wing: Shrinkage and displacement influenced by an induced magnetic field. *Annales Geophysicae*, *25*(4), 905–914. <https://doi.org/10.5194/angeo-25-905-2007>
- Zimmer, C., Khurana, K. K., & Kivelson, M. G. (2000). Subsurface oceans on Europa and Callisto: Constraints from Galileo magnetometer observations. *Icarus*, *147*(2), 329–347. <https://doi.org/10.1006/icar.2000.6456>